Scalable Green Sustainable Photosynthesis of H_2O_2: Catalyst-free H Radical Generation and ORR Under Sunlight

Meng Liu[a], Qi Miao[b], Xiaoyuan Zhou[a], Dan Luo[a], Hongli Wei[a], Pan Wu[a], Chang-jun Liu[a], Wei Jiang[a]*

[a]Low-carbon Technology and Chemical Reaction Engineering Laboratory, School of Chemical Engineering, Sichuan University, Chengdu, 610065 (PR China)

[b]Tsinghua Shenzhen International Graduate School, Tsinghua University, Shenzhen 518055, P. R. China

E-mail: weijiang@scu.edu.cn

Sichuan University, No.24 South Section 1, Yihuan Road

College of Chemical Engineering

Table of Contents

General Remarks

All commercially available compounds were purchased from Greagent, DOJINDO and Adamas-beta. 1-phenylethanol (PA) (98%), benzyl Alcohol (BA) (99%), Diphenylmethanol (DPM) (99%), Benzophenone (BP) (99%), Ethyl Acetate (EA) (99%), Toluene (99.5%) and Ethanol (95%) were purchased from Adamas-beta. Dichloromethane (DCM) (99.5%) was purchased from Greagent. 5,5-dimethyl-1-pyrroline-1-oxide (DMPO) was purchased from DOJINDO.

Figure S1

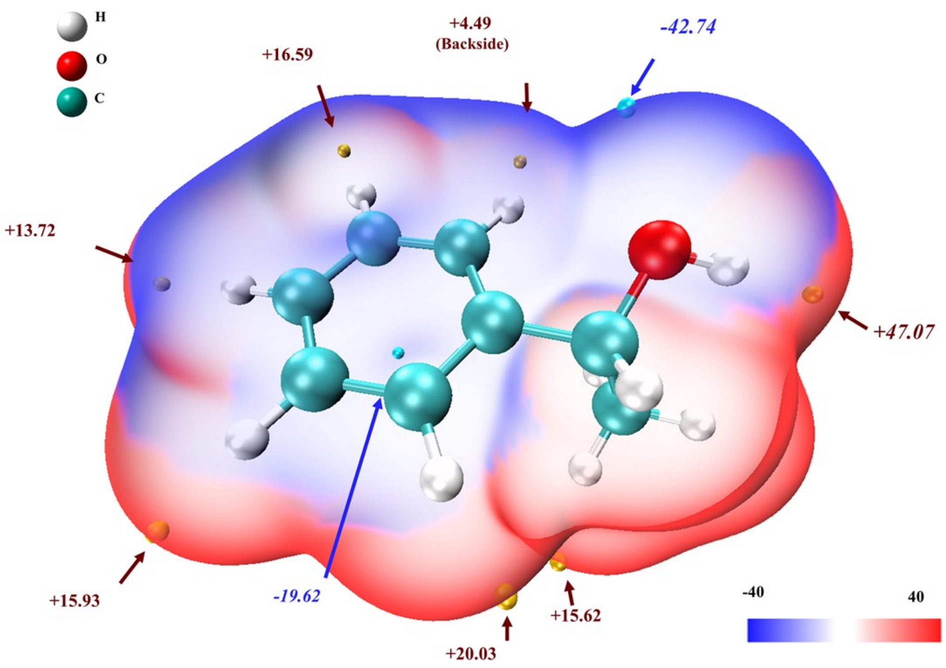

Supplementary Fig. S1 ESP mapped vdW surface (namely, isosurface of r ¼ 0.001 au) of the PA. (Values of ESP at the surface extrema are labelled from blue to red. Units are in kcal/mol. Cyan and orange spheres correspond to ESP minima and maxima on the surface)

ESP is usually studied on the vdW surface defined as an electron density (r) equal to 0.001 au[1, 2]. For the reason that the molecular ESP on this surface sufficiently reflects the possible electrostatic interaction between a molecule and other molecules and is closely related to intermolecular electrostatic interaction energy, quantitative molecular surface analysis was carried out to study interactions driven by electrostatics effect. The extrema of the ESP distributed on the vdW surface of the PA are represented as cyan and orange spheres in Fig. S1. The PA maxima of the ESP is +47.07 kcal/mol, which represented as orange is closed to H atom of O-H, and the minima of the ESP shown as cyan is closed to the O atom of O-H (-42.74 kcal/mol). The above results indicate that hydrogen group is more active and tends to participate in reaction.

Figure S2

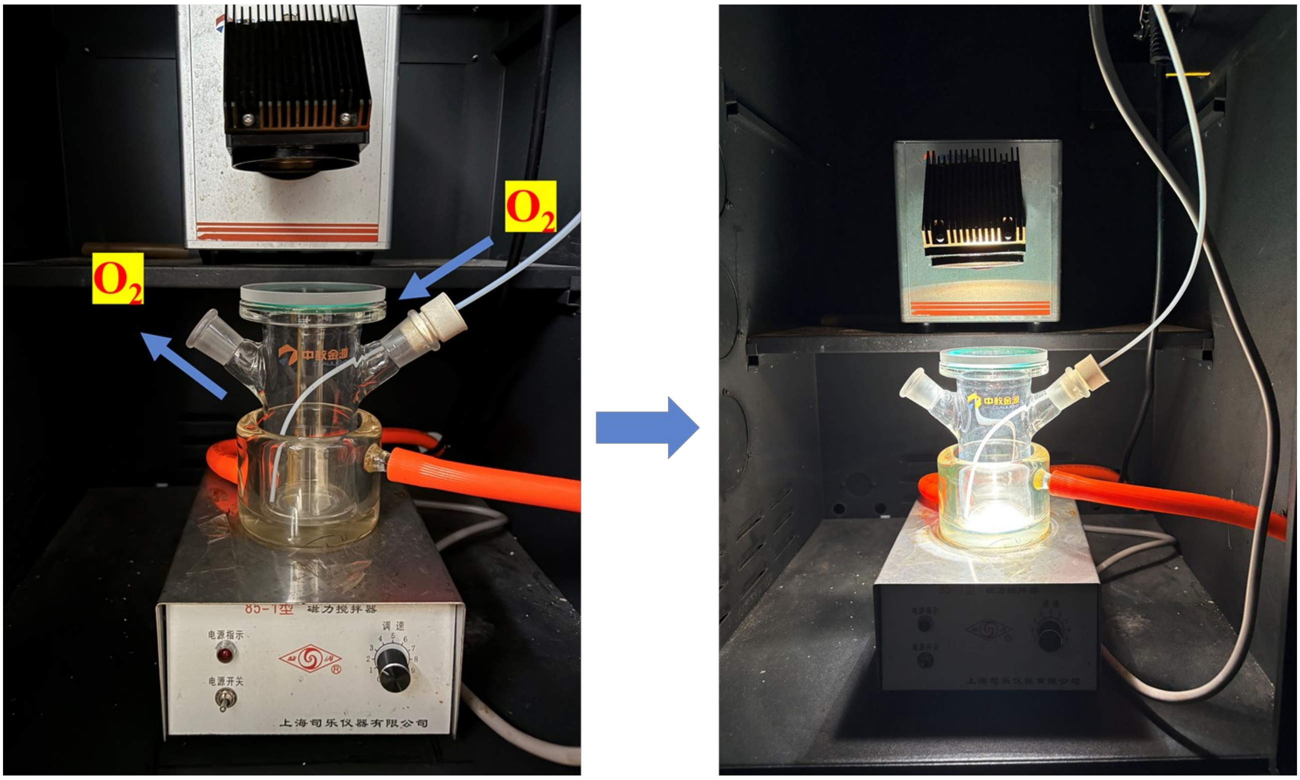

Supplementary Fig. S2 The pre-experiments using PA for direct catalyst-free H_2O_2 photosynthesis. a) Oxygen in the tube ; b) The DPM system was irradiated by Xe lamp

As shown in **Fig. S2**, the pre-experiments using PA as the substrate for direct H_2O_2 photosynthesis without catalyst based on the conditions of 5 mL of PA, maintaining an O_2 atmosphere at a temperature of 20 °C, along with Xe lamp irradiation (λ = 300-1000 nm) (**b**). After 4 hours, the reaction solution is extracted with 25ml H_2O for 3 minutes to separate H_2O_2 from the oil phase. The H_2O_2 yield reaches a significant concentration of 212 mM with a corresponding reaction rate of 128.83 mM·h^{-1}, which is far better than BA (double BA's output (112.30 mM).

Figure S3

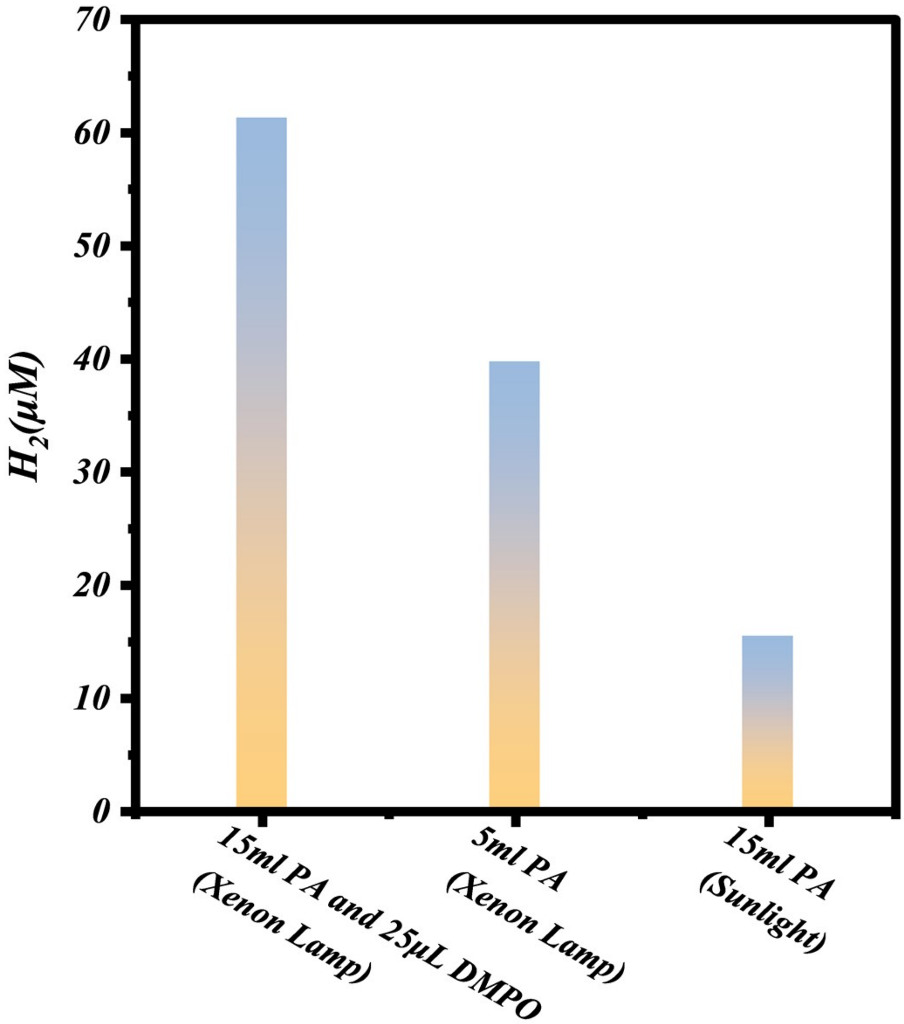

Supplementary Fig. S3 PA photosynthesizes H_2 (5 h): (I) PA (15 mL) mixed with DMPO (25 μL), N_2 (1 atm) at 20 °C, xenon lamp irradiation (λ = 300–780 nm); (II) PA (5 mL), N_2 (1 atm) at 20 °C, xenon lamp irradiation (λ = 300–780 nm); (III) PA (15 mL), N_2 (1 atm) at 20 °C, natural sunlight irradiation on March 12, 2025.

As shown in **Fig. S3**, when 5,5-dimethyl-1-pyrroline N-oxide (DMPO), a radical scavenger, was added to PA, the H_2 yield increased unexpectedly. This may be attributed to the preferential capture of benzyl radicals (**RCOH•**) by DMPO, resulting in the rapid consumption of uncaptured active **H•** to produce H_2[9-11]. This result confirms that H_2 production is the main side-reaction in the H-ORR process. The synchronous decrease in the two products indicates that some post-reactions exist, which may be the further deep oxidation of ACP and the consumption/self-decomposition of H_2O_2. This is owing to the excessively high concentrations of H_2O_2 and ACP, which inhibit the main reaction, causing product consumption.

Figure S4

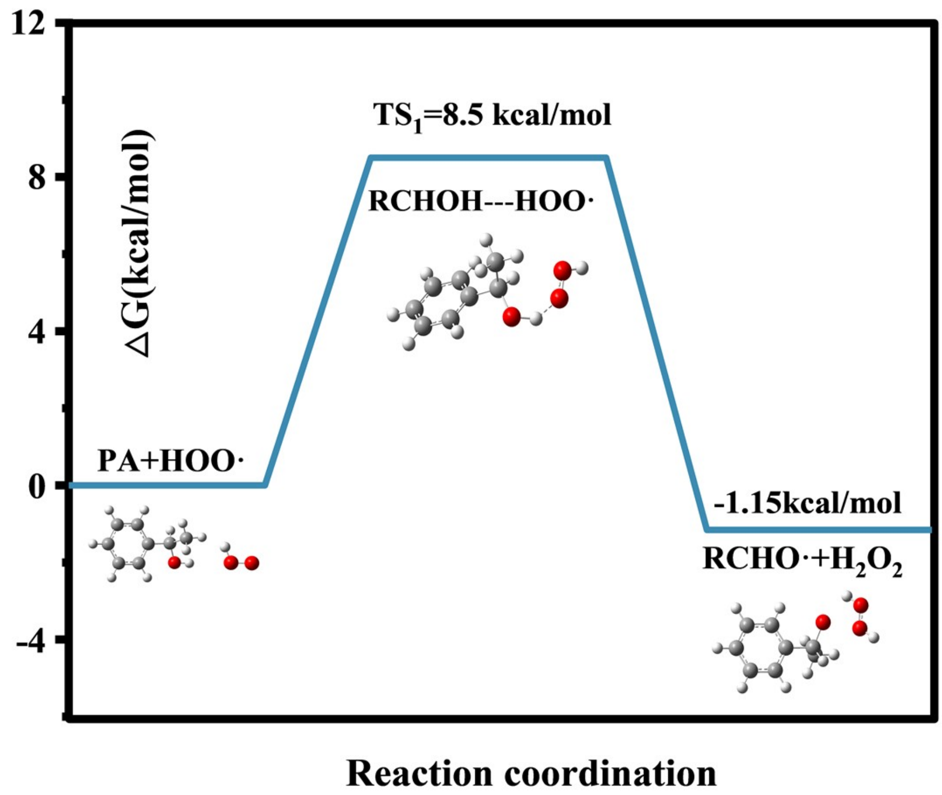

Supplementary Fig. S4 The transition states and energy barriers of unexcited PA and HOO· with B3LYP-D3/6-311++G (d, p) method.

As shown in **Fig. S4**, the transition states of HOO• and unexcited PA is studied by B3LYP-D3/6-311++G (d, p) method. Free HOO• shows electrostatic interaction with PA under hydrogen effect. Then active HOO• capture the H atom of OH group in TS_1 process and finally forming H_2O_2 and RCHO•. The small energy barrier of TS_1 is 8.5kcal/mol and the reaction is exothermic with decreasing free energy. Thus the reaction of HOO• and unexcited PA is thermodynamically feasible.

Figure S5-8

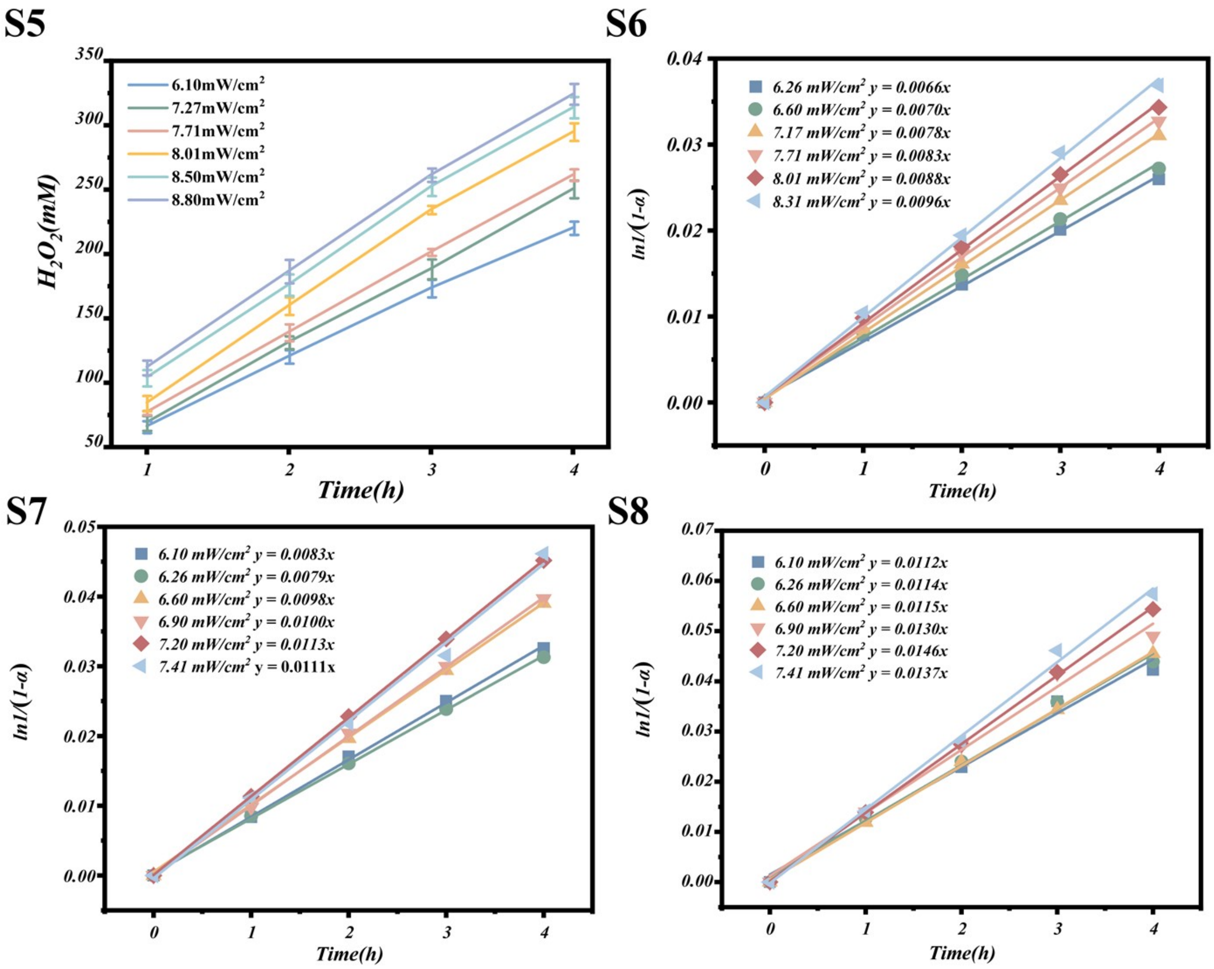

Supplementary Fig. S5-8 The first-order kinetic fitting of light intensity-dependent H_2O_2 formation.

Follow by linear relationship between ln(1/1-α) and time also proved. Followed by the Temperature-dependent reaction rate constants derived from the Arrhenius equation (as the follows):

$$k = Ae^{-Ea/RT}$$

Taking the logarithm of the formula gives:

$$lnk = \frac{-Ea}{RT} + lnA$$

As shown in article Table 3, lnk_T and $1/T$ have a good linear relationship, the reaction rate constant(k_T) of temperature is derived based on the logarithm of Arrhenius formula:

$$k_T = e^{(3.6116 - \frac{2541.5}{T})}$$

Temperature and light favor radical homolysis, and the actual H_2O_2 yield is almost proportional to the light intensity with ratio of 0.4575, which is almost equal to the determined AQY value. Therefore, the simple relationship between the reaction rate constant *(R)* of H-ORR, the temperature *(T)* and light intensity *(I)* are follows:

$$R = k_0 * AQY * I * k_T * C$$

substituting k_T into R gives:

$$R = k_0 * AQY * I * e^{\left(3.6116 - \frac{2541.5}{T}\right)} * C$$

Then the relationship between different light intensity and reaction rate constants was investigated under the temperature conditions 30℃ and 40℃, respectively, as shown in Fig. S5-8. It is found that the reaction rate constant and light intensity at different temperatures have a good linear relationship. The increase of light intensity on the photoreaction was evaluated. The H_2O_2 concentration in PA further increased from 220.50 to 319.97 mM when intensity of the light source (λ=313 nm) was increased from 6.10 to 8.80 $mW \cdot cm^{-2}$, respectively (Fig.S5). This linear relationship between the actual H_2O_2 yield and the light intensity with a coefficient of 0.4575 indicated a constant AQY value for the H-ORR process.and the k values of different temperatures are 0.3676 and 0.3817, respectively, and the average value is 0.3779. The final reaction rate equation about light intensity and temperature is as follows:

$$R = k_0 * AQY * I * e^{\left(3.6116 - \frac{2541.5}{T}\right)} * C$$

$$(k_0 \approx 0.3779)$$

Figure S9

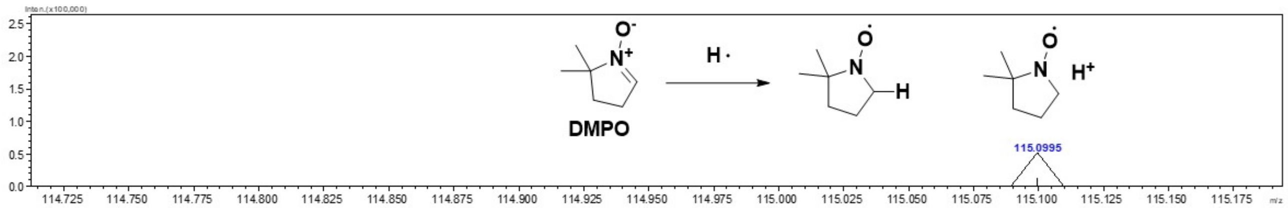

Supplementary Fig. S9 Under Ar conditions the adduct of the H• and DMPO detected by high-resolution mass spectroscopy (HRMS) with PA.

To gain the adduct of the H• intermediate and DMPO, the experiments based the condition of PA (3 mL), mixed with DMPO (25 μL), consequent Ar (1 atm) at 20℃, irradiation of a xenon lamp (λ= 300-1000 nm) was performed. 5 minutes later, the adducts of H• and DMPO was detected by High-resolution mass spectra (**HRMS** *m/z* (ESI) calculated for $[C_6H_{12}NO\bullet+H^+]^+$115.0992, found 115.0995).

Figure S10

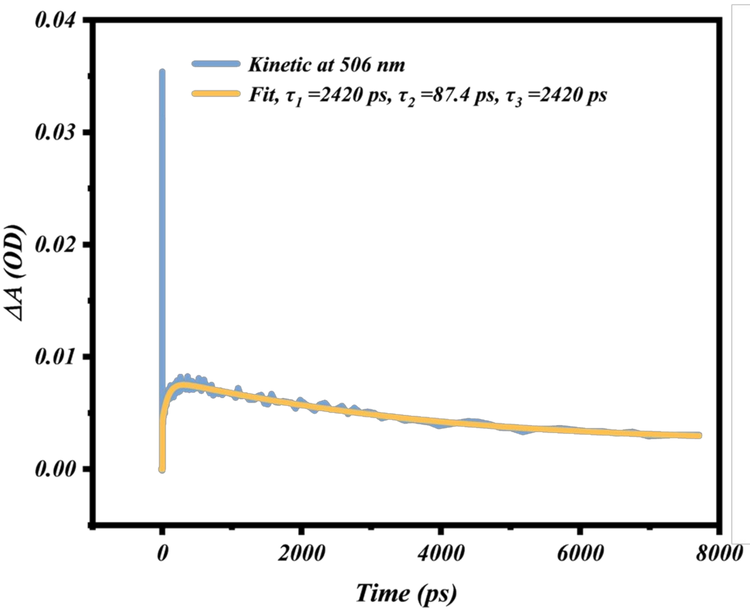

Wavelength	506nm
t_0	4
IRF	0.14ps
A_1	0.5
t_1	2420ps
A_2	-1.09E-6
t_2	87.4ps
A_3	0.5
t_3	2420ps
A_4	7e-7
t_4	Inf

Supplementary Fig. S10 The Kinetic fitting results of PA under oxygen-free conditions at 506 nm.

In order to investigate the kinetic of PA corresponding to the blue blunt peaks **(Fig. 6d)** under oxygen-free conditions, a kinetic fitting study was performed of PA at a wavelength of 506 nm. The results as shown in **Fig. S10**, the yellow blunt peak may mainly include three kinetic processes, and two of which are equal. Thus, two slow processes of equal duration (approximately 2420 ps), namely the picosecond level PA hydroxy O-H homolysis for RO• and H• generation. The intramolecular hydrogen atom transfer (HAT) and the recombination from benzyl to hydroxyl group (RCOH•) with 87.4ps assigned. It can be supposed that there are two forms radicals of RO• and RC• radicals co-exists after detaching a H•. When **H•** reacts with the C site of the RO• form, the recombination occurs; when **H•** transfer to O group of the **ACP** form, H_2 generates, and the residue part of dehydrogenated **RCO•** converts to ACP.

Figure S11

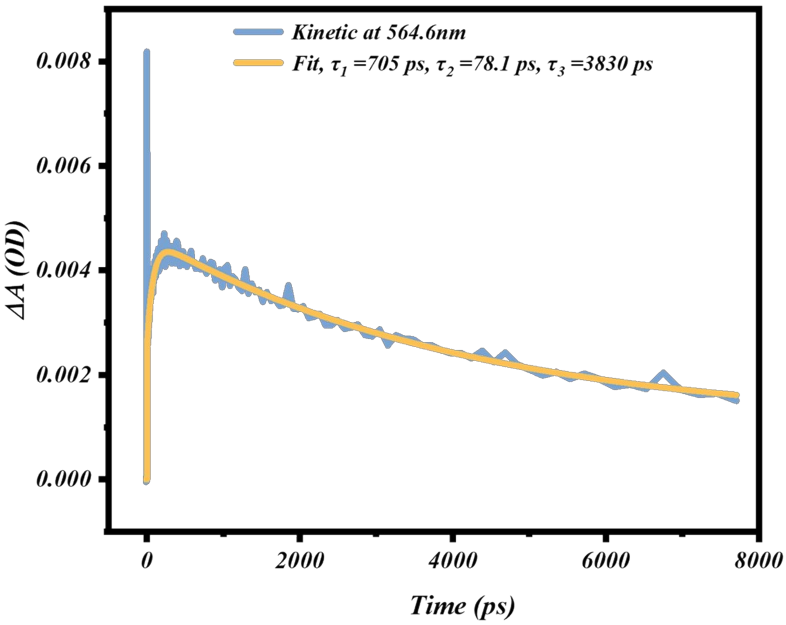

Wavelength	564.6 nm
$\mathbf{t_0}$	3.001
IRF	0.14 ps
$\mathbf{A_1}$	-0.0107
$\mathbf{t_1}$	705 ps
$\mathbf{A_2}$	-0.301
$\mathbf{t_2}$	78.1 ps
$\mathbf{A_3}$	0. 516
$\mathbf{t_3}$	3830 ps
$\mathbf{A_4}$	0.172
$\mathbf{t_4}$	Inf

Supplementary Fig. S11 The kinetic fitting results of PA under oxygen conditions at 564.6 nm.

In order to investigate the kinetic of PA corresponding to the blue blunt peaks under oxygen conditions, a kinetic fitting study was performed at a wavelength of 564.6 nm. The results as shown in **Fig. S11**, the blunted blue peaks exhibit a 705 ps process and a secondary 78.1 ps processes. Compared the first process with 2420 ps in S9, the rapidly shortened reaction time 705 ps process was inferred to be the efficient OR• O-H homolysis cleavage, indicating that active O_2 can strongly capture free H• and promote the O-H homolysis. The 78.1 ps process was inferred to be the HAT process and the recombination from benzyl for **RO•** generation, which was equal to that under oxygen-free condition (87.4 ps), indicating that HAT process is a very rapid femtosecond-level response. The HAT and **RO•** generation are easily spontaneous. O_2 mainly has effect on benzylic C-H homolytic cleavage.

Figure S12

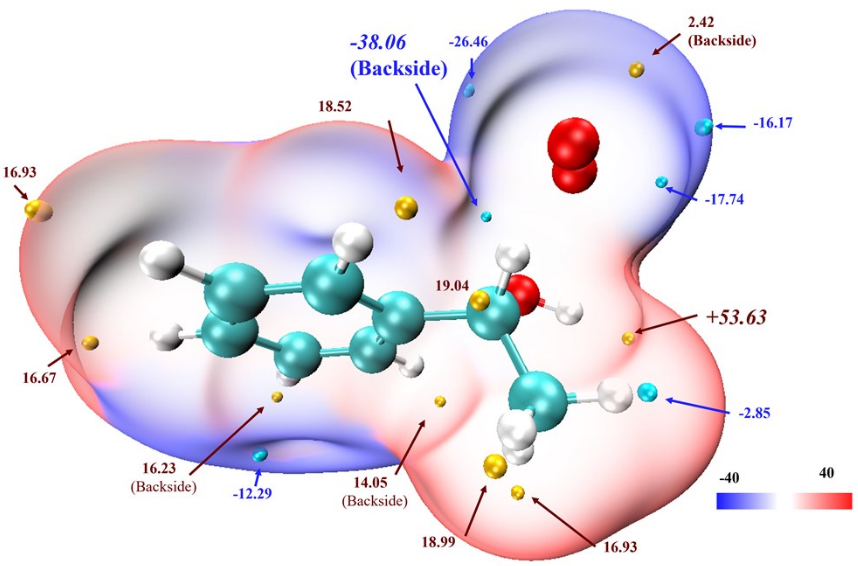

Supplementary Fig. S12 ESP mapped vdW surface of the PA-O_2. (Values of ESP at the surface extrema are labelled from blue to red. Units are in kcal/mol. Cyan and orange spheres correspond to ESP minima and maxima on the surface).

As shown in **Fig. S12**, ESP is usually studied on the vdW surface defined as an electron density (r) equal to 0.001 au[1, 2]. For the reason that the molecular ESP on this surface sufficiently reflects the possible electrostatic interaction between a molecule and other molecules and is closely related to intermolecular electrostatic interaction energy, quantitative molecular surface analysis was carried out to study interactions driven by electrostatics effect. The PA-O_2 maxima of the ESP is +53.63 kcal/mol, which represented as orange is closed to H atom of O-H, and the minima of the ESP shown as cyan is closed to the O atom of O-H (-38.06 kcal/mol). The following negative ESP surface is around O_2, which attributes to forming amounts hydrogen bonds of H-O_2. O_2 could strongly interact with hydrogen group and form stable PA-O_2 with strongly electrostatic interaction. Compared with PA in Fig.S1(which maxima is +47.07 kcal/mol), the presence of O_2 could enhance surface polarity.

Figure S13

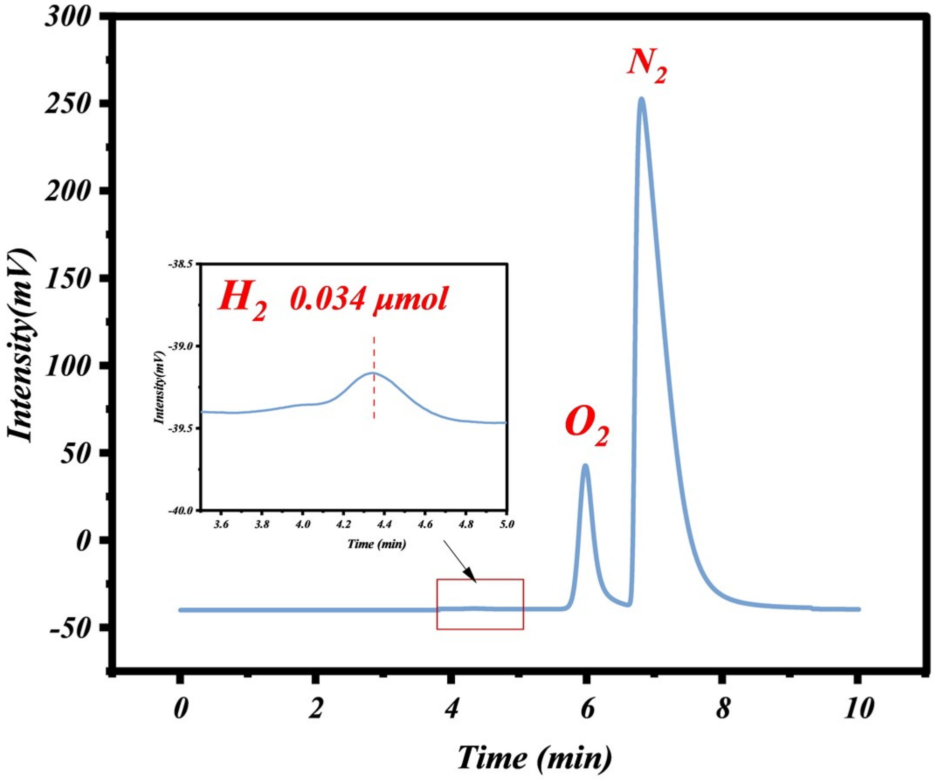

Supplementary Fig. S13 Gas chromatography (GC) results of PA (5 mL) under oxygen conditions with Xe lamp irradiation (λ = 300-1000 nm).

As shown in **Fig. S13**, The H_2 production was measured by a gas chromatography analyzer (Agilent Micro-GC). the PA photosynthesizes H_2O_2 experiment is PA (15 mL) with continuous delivery O_2 at 20 °C, xenon lamp irradiation (λ = 300–780 nm) with 4 hours. **0.034** μmol H_2 is detected. The result indicates that under aerobic conditions, trace amounts of H_2 are still generated.

Figure S14

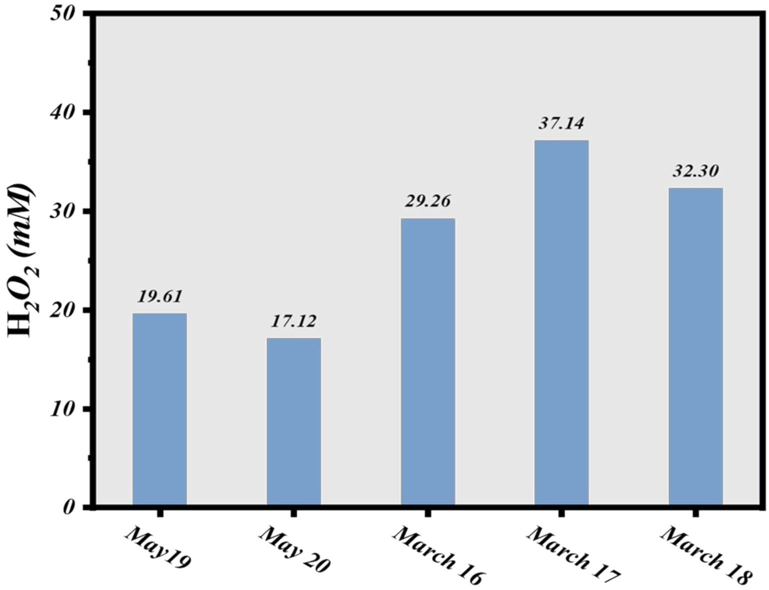

Supplementary Fig. S14 The H_2O_2 concentration under different weather conditions in 2025

As shown in **Fig. S14**, five typical all-weather experiments are studied including sunny, cloudy and rainy days in 2025. The sunshine time was about 6-7 hours and the sunlight intensity fluctuated from 1 to the maximum value, more than 100 klx.

Figure S15

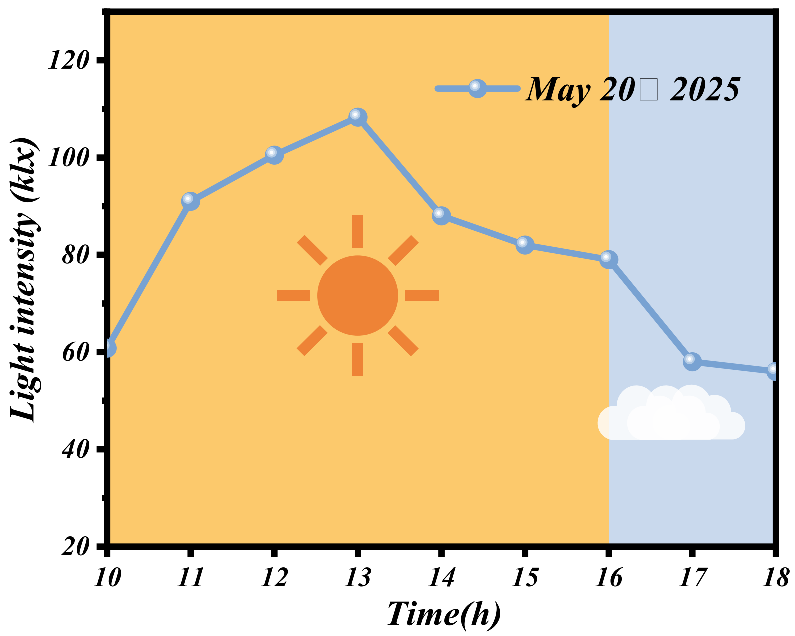

Supplementary Fig.S15. The H_2O_2 production on a sunny day (May 20, 2025)

As shown in **Fig. S15**, the sunshine time was 10:00–16:00 on May 20, 2025, and the sunlight intensity fluctuated from 62.15 to the 109.73 klx, then began to drop rapidly after 16 pm, the measured light intensity obeying the principles of nature. After 6 h of irradiation, the H_2O_2 yield was 17.12mM in 40 mL of PA with an irradiated area of 193 cm^2.

Figure S16

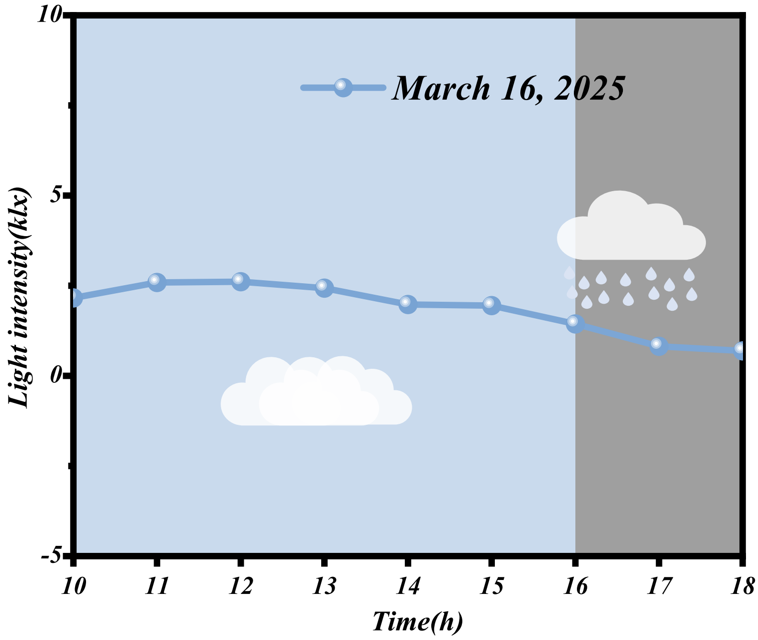

Supplementary Fig.S16 The H_2O_2 production on a windy day (March 16, 2025)

As shown in **Fig. S16**, the sunshine time was 10:00–16:00 on March 16, 2025, and the sunlight intensity fluctuated from 2.47 to the 1.61 klx. The measured light intensity obeying the principles of nature. After 6 h of irradiation, the H_2O_2 yield was 29.26 mM in 40 mL of PA with an irradiated area of 193 cm^2.

Figure S17

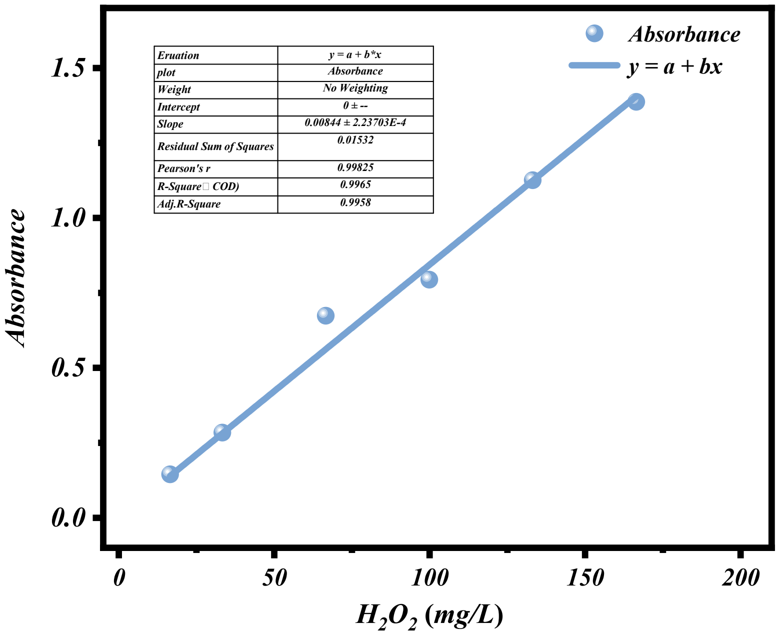

Supplementary Fig. S17 The standard curve for hydrogen peroxide.

As shown in **Fig. S17**, the UV-Vis absorbance peaks of H_2O_2 were monitored at wavelengths of 400 nm for concentrations of 166.43 mg/L, 133.14 mg/L, 99.86 mg/L, 66.57 mg/L, 33.29 mg/ and 16.49 mg/L. A linear regression equation was constructed, enabling quantification of the amount of H_2O_2 in unknown samples based on their signal values.

Figure S18

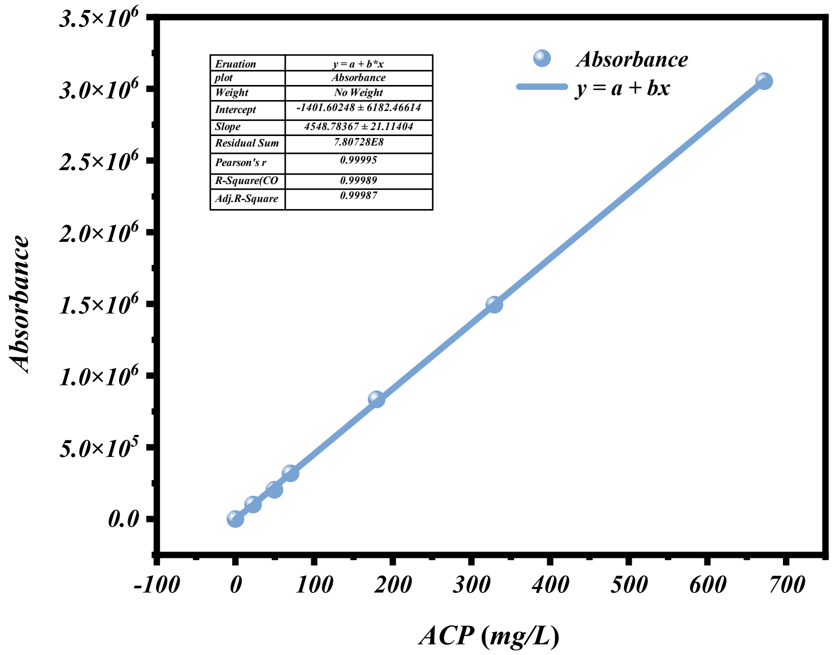

Supplementary Fig. S18 The standard curve for Acetophenone.

As shown in **Fig. S18**, the absorbance peaks of Acetophenone (ACP) were monitored by high-performance liquid chromatography (HPLC) at wavelengths of 241 nm for concentrations of 672.18 mg/L, 329.08 mg/L, 179.41 mg/L, 70.12 mg/L, 49.50 mg/L and 22.37 mg/L. A linear regression equation was constructed, enabling quantification of the amount of ACP in unknown samples based on their signal values. This standard curve exhibited a high degree of linearity and sensitivity, demonstrating its suitability for accurate and precise quantification of acetophenone in a variety of samples.

Figure S19

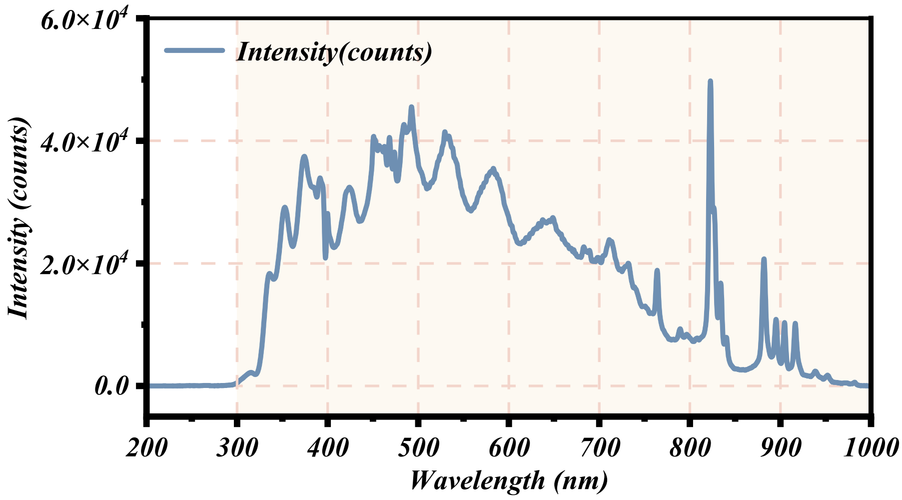

Supplementary Fig. S19 The full spectrum of xenon lamp.

As shown in **Fig. S19**, it exhibits the full spectrum of a xenon lamp used in our experiments. It can be found that the light with wavelength less than 300 nm is not provided. The main spectrum region is between 300 nm and 980 nm, and mainly concentrates between 350 nm and 760 nm, the visible light region. Only a little UVA light from 310 nm to 400 nm, is supplied by this xenon lamp.

Table S1

Using (D3) B3LYP-D3/6-311++G(d, p)[3-5] to calculate the electronic transition energy of singlet PA as well as the comparison between the experimental and calculated values of the absorption wavelength, the electronic transition orbit and the transition properties[6-8], the calculation results are shown in **Table S1**. It can be seen that PA-O_2 has a strong absorption band at 241 nm, and the orbital transitions corresponding to the S1 state of PA are mainly 33-34 orbitals and belongs to the $\pi_H \rightarrow \pi_L^*$ transition. The molecular orbitals are mainly distributed in the benzene ring before excitation, and electrons are transferred from the benzene ring to the hydroxyl and benzylic C-H bonds after excitation, which makes the electronic properties of O-H and C-H more active. Thus, PA tend direct homolysis cleavage to form radical pairs. This result is consistent with the small ΔG_1 of TS_1 results in Fig.2.

Table S1. Calculation conditions of B3LYP-D3/6-311++G(d, p) and experimentally obtained electron orbital transition energies and absorption wavelengths of PA

States	Character	Singlet transition energies			Orbitals
		Expt.	Calc.	Calc.	
S1	$\pi_H \rightarrow \pi_L^*$	241 nm	233 nm	5.305 eV	33→34

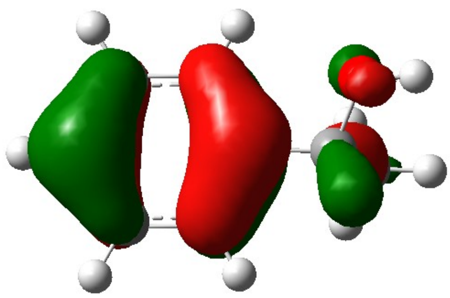

33: π_H

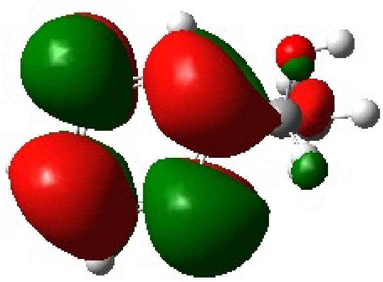

34: π_L^*

Table S2

Using (D3) B3LYP-D3/6-311++G (d, p)[3-5] to calculate the electronic transition energy of singlet PA-O_2 as well as the comparison between the experimental and calculated values of the absorption wavelength, the electronic transition orbit and the transition properties[6-8], the calculation results are shown in **Table S1**. It can be seen that PA has a strong absorption band at 321 nm, which close to the experiment of 326 nm in Fig.7a. The orbital transitions corresponding to the S1 state of PA-O_2 are mainly 41-42 orbitals and belongs to the $\pi_H \rightarrow \pi_L^*$ transition. After excitation, the molecular HOMO orbital is mainly distributed on the O=O, and electrons are transferred from the O=O to the hydroxyl O-H bonds at LUMO orbital, which makes the electronic properties of O-H more active. Thus, PA-O_2 may could direct homolysis cleavage to form **HOO•** pairs. This result is consistent with the detection of **HOO•** and **RO•** under O_2 atmosphere in Fig.6, the surface ESP results in Fig.S12 and ΔG_1 of TS-1 results in Fig.7d.

Table S2. Calculation conditions of B3LYP-D3/6-311++G(d, p) and experimentally obtained electron orbital transition energies and absorption wavelengths of PA-O_2

States	Character	Singlet transition energies			Orbitals
		Expt.	Calc.	Calc.	
S1	$\pi_H \rightarrow \pi_L^*$	329 nm	326 nm	3.769 eV	41→42

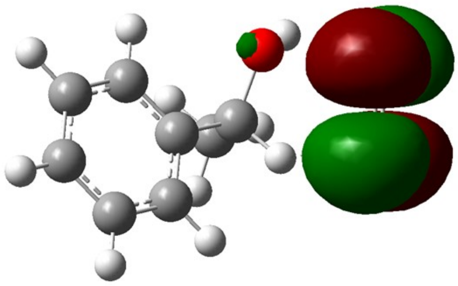

41: π_H

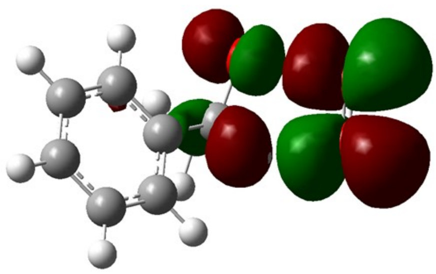

42: π_L^*

Table S3

Table S3. Comparation product and green sustainability metrics of PA (this work, catalyst-free), BA[12] (our prior work, catalyst-free), BA[13] (our prior work, g-C_3N_4), Water[14](advanced report, C_3N_5-KNO_3) traditional industrial anthraquinone[15] (AQ) method based H_2O_2 production. (Based on 1L reactant)

		Catalyst-free H_2O_2 production			**Photocatalysis H_2O_2 production**		**Traditional AQ**
		This work (Catalyst-free PA)		**Our previous work (Catalyst-free BA)**	**Our previous work (BA)**	**Advanced report (10% ethanol)**	
		Sunlight	Artificial light	Artificial light	Artificial light	Artificial light	
Product	Yield (mM/h)	3.34	12.69	6.236	2.36	1.55	131.1
	Concentration (mM)	23.35	216.20	149.67	70.93	2.32	199.50
Green Methods	Oxidation	All-weather Sunlight	300 W Xenon lamp	300 W Xenon lamp	300 W Xenon lamp	300 W Xenon lamp	55°C/ 0.3Mpa
	Catalysts/sacrifice	/	/	/	g-C_3N_4/BA	C_3N_5-KNO_3/EA	/
	Extraction/Back-Extraction	H_2O/Sunlight	H_2O/oil	No-re	H_2O/oil	No-re	H_2O/oil
	Reduction	Pd_{np}-g-C_3N_4+H_2O	Raney Ni+H_2	Pd/ZrO_2+H_2	No report	No report	Pd/Al_2O_3+H_2
Green Metrics	By-product	ACP (sole product)		BD, BC and BZ	BD, BC and BZ	Aldehyde	AQ, HAQ and potential polymers after deep oxidation
	Waste stream	Condensation reuse		reuse	BD excretion	No report	heavy oil and excessive oxidation
	Waste water	Re-extraction solution with less COD (RES)		Re-extraction solution with less COD	re-extraction solution with less COD	No report	Excessive oxidation products and heavy oil
	Catalyst loss in ORR	/	/	/	Mass lose	Mass lose	Mass lose
	Catalyst loss in hydrogenation	Negligible		Negligible	No report	No report	Negligible
	Corrosion	Slight		Slight	No report	No report	Severe by liquid
	Toxicity /volatility	LD_{50}=2820/3200/slight		LD_{50}=1230/low	LD_{50}=1230/low	No-re	LD_{50}=2000 /highly

To ensure the article meets initial publication standards and looks nice, some of the content in table 5 has been shortened. Here's a detailed explanation of the abbreviations used: the AQ means anthraquinone, HAQ means hydroanthraquinone. In product part, AL means artificial light. In Green Methods part, 300Wmeans 300 W Xenon lamp, EA means ethanol, No-re means this research has not reported the related research. In Green Metrics part, Mix heavy oil means heavy oil, excessive oxidation and potential polymers after deep oxidation, RES means re-extraction solution with less COD, loss means catalyst mass loss. Toxicity shows as the $LD_{50.}$ LD_{50} > 2000 mg·kg^{-1} is classified as 'low toxicity', while 500–2000 mg·kg^{-1} of LD_{50} is classified as 'moderately toxic'.

References

1. Z. Liu, T. Lu and Q. Chen, *Carbon*, 2020, **165**, 461-467.
2. T. Lu and S. Manzetti, *Structural Chemistry*, 2014, **25**, 1521-1533.
3. J.-H. Li, J.-D. Chai, G.-Y. Guo and M. Hayashi, *Chemical Physics Letters*, 2011, **514**, 362-367.
4. P. V. Ramana, T. Sundius, S. Muthu, K. C. Mouli, Y. R. Krishna, K. V. Prasad, R. N. Devi, A. Irfan and C. Santhamma, *Journal of Molecular Structure*, 2022, **1253**, 132211.
5. S. J. Freakley, Q. He, J. H. Harrhy, L. Lu, D. A. Crole, D. J. Morgan, E. N. Ntainjua, J. K. Edwards, A. F. Carley, A. Y. Borisevich, C. J. Kiely and G. J. Hutchings, *Science*, 2016, **351**, 965-968.
6. I. S. Kritchenkov, D. D. Zhukovsky, A. Mohamed, V. A. Korzhikov-Vlakh, T. B. Tennikova, A. Lavrentieva, T. Scheper, V. V. Pavlovskiy, V. V. Porsev, R. A. Evarestov and S. P. Tunik, *Bioconjugate Chemistry*, 2020, **31**, 1327-1343.
7. S. Nayeri, S. Jamali, V. V. Pavlovskiy, V. V. Porsev, R. A. Evarestov, K. S. Kisel, I. O. Koshevoy, J. R. Shakirova and S. P. Tunik, *European Journal of Inorganic Chemistry*, 2019, **2019**, 4350-4357.
8. M. Li, W. Harrison, Z. Zhang, Y. Yuan and H. Zhao, *Nature Chemistry*, 2024, **16**, 277-284.
9. Y. Shiraishi, S. Kanazawa, Y. Kofuji, H. Sakamoto, S. Ichikawa, S. Tanaka and T. Hirai, *Angewandte Chemie International Edition*, 2014, **53**, 13454-13459.
10. H. Wang, C. Yang, F. Chen, G. Zheng and Q. Han, *Angewandte Chemie International Edition*, 2022, **61**, e202202328.
11. Y. Shiraishi, S. Kanazawa, D. Tsukamoto, A. Shiro, Y. Sugano and T. Hirai, *ACS Catalysis*, 2013, **3**, 2222-2227.
12. H. Zhang, M. Liu, Q. Miao, P. Wu, C. Liu and W. Jiang, Chemical Engineering Journal, 2023, **455**, 140649.
13. H. Zhang, M. Liu, X. Zhang, B. Yuan, P. Wu, C. Liu and W. Jiang, Chemical Engineering Journal, 2022, **438**, 135664.
14. S. Jing, Q. Xu, H. Wang, P. Kannan, H. Liang, A. Brouzgou, R. Wang and P. Tsiakaras, Journal of Colloid and Interface Science, 2025, **695**, 137675.
15. Y. J. Zhang, Q, Lv, X. B. Li, L. Li, Journal of nanjing University, 2023, **59(3)**: 494-502.